J. Fluid Mech. (2002), *vol.* 452, *pp.* 145–162.
DOI: 10.1017/S0022112001006693 Printed in the United Kingdom

Inertially driven inhomogeneities in violently collapsing bubbles: the validity of the Rayleigh–Plesset equation

By HAO LIN[1], BRIAN D. STOREY[2] AND ANDREW J. SZERI[1]

[1]Department of Mechanical Engineering, University of California, Berkeley, CA 94720-1740, USA

[2]Franklin W. Olin College of Engineering, Needham, MA 02492-1245, USA

(Received 11 December 2000 and in revised form 6 August 2001)

When a bubble collapses mildly the interior pressure field is spatially uniform; this is an assumption often made to close the Rayleigh–Plesset equation of bubble dynamics. The present work is a study of the self-consistency of this assumption, particularly in the case of violent collapses. To begin, an approximation is developed for a spatially non-uniform pressure field, which in a violent collapse is inertially driven. Comparisons of this approximation show good agreement with direct numerical solutions of the compressible Navier–Stokes equations with heat and mass transfer. With knowledge of the departures from pressure uniformity in strongly forced bubbles, one is in a position to develop criteria to assess when pressure uniformity is a physically valid assumption, as well as the significance of wave motion in the gas. An examination of the Rayleigh–Plesset equation reveals that its solutions are quite accurate even in the case of significant inertially driven spatial inhomogeneity in the pressure field, and even when wave-like motions in the gas are present. This extends the range of utility of the Rayleigh–Plesset equation well into the regime where the Mach number is no longer small; at the same time the theory sheds light on the interior of a strongly forced bubble.

1. Introduction

In applications such as ultrasonic imaging, shock wave lithotripsy, sonochemistry, and sonoluminescence, micron sized bubbles are forced into radial oscillations by pressure waves in the surrounding medium. Bubbles under these conditions typically undergo long slow expansions and violent collapses. The collapse compresses the bubble rapidly, with the consequence that the contents can reach temperatures extreme enough to emit light (sonoluminescence). Significant gas-phase chemical reactions can occur in the bubble interior (relevant to sonochemistry).

The general behaviour of the bubble oscillations can be captured by the Rayleigh–Plesset equation: a nonlinear ODE derived from the Navier–Stokes equations of the liquid under the assumption of spherical symmetry. In order to close the Rayleigh–Plesset equation, one usually assumes that the gas in the bubble has uniform pressure and undergoes on average a polytropic thermodynamic process. It is an accepted notion by some researchers that if the (gas) Mach number of the bubble wall is not small then the pressure field in the bubble will be non-uniform (Putterman *et al.* 2001);

in this case the gas dynamics is expected to be characterized by wave-like motion. The pressure field in the bubble, the nature of the gas dynamics, and the formation of shock waves have been the subject of a number of studies including Chu (1996), Greenspan & Nadim (1993), Kwak & Na (1997), Lin & Szeri (2001), Prosperetti, Crum & Commander (1988), Prosperetti (1991), and Vuong, Szeri & Young (1999), among others.

In spite of this conjectured correlation between the Mach number and the pressure non-uniformity, the 'uniform [pressure] bubble model appears to be quite successful in describing the basic facts' of sonoluminescence (Hammer & Frommhold 2001), even when Mach number is not small. Earlier researchers made attempts to give an explanation from an acoustical perspective (Trilling 1952), whereas in this work we explore the inhomogeneity of the bubble from a hydrodynamic view.

Based on the present analysis and on an examination of detailed simulations of the gas dynamics in the bubble interior, we have concluded that there is much evidence to challenge the importance of the Mach number in judging the expected spatial uniformity of the pressure field. In the case of violently collapsing microbubbles, we shall argue that the Mach number is not the distinguishing parameter, due to the relatively small size of the bubble compared to a pressure wavelength we define below. Compression waves in a small confined domain behave rather differently than in a semi-infinite domain: a geometry in which use of the Mach number (and much of one's intuition) is based. Instead, we shall derive a dimensionless acceleration whose smallness is directly related to the uniformity of the pressure field in the bubble. The dimensionless acceleration is involved in an expression for a spatially non-uniform pressure field. We find this expression to be quite accurate when compared with detailed numerical simulations. Also developed are the criteria to judge the validity of the uniform pressure assumption as well as the non-uniform pressure solution. When these criteria are violated one can anticipate wave-like gas dynamics. The analysis presented in this paper greatly extends the range of parameter space where the classical Rayleigh–Plesset equation (RPE) is useful, at least with respect to the uniform pressure assumption.

The plan of the paper is as follows. In §§ 2–4, we develop the approximation for inertially driven inhomogeneity in the pressure field, and compare the approximate pressure fields to DNS. In § 5, we discuss the consequences of heat transfer. In § 6, we explore the changes that result in solutions of the RPE if one uses the non-uniform pressure approximation to close the equation rather than the customary spatially uniform pressure approximation. Finally, in § 7 we identify different regimes of bubble dynamics, and summarize our findings concerning the physical validity and quantitative accuracy of the uniform pressure closure of the RPE.

2. The dimensionless quantity ϵ_p

We start with a heuristic derivation of a dimensionless time-dependent acceleration that will serve as an indicator for pressure non-uniformity. Its utility will be considered in the following sections.

We begin with the Euler equations as the governing equations for the gas in a bubble assuming spherical symmetry:

$$\frac{1}{\rho}\left(\frac{\partial \rho}{\partial t} + v\frac{\partial \rho}{\partial r}\right) + \frac{\partial v}{\partial r} + \frac{2v}{r} = 0, \tag{2.1}$$

$$\rho\left(\frac{\partial v}{\partial t}+v\frac{\partial v}{\partial r}\right)=-\frac{\partial p}{\partial r}, \tag{2.2}$$

$$\frac{p}{\rho^k}=\text{constant}. \tag{2.3}$$

Here ρ is the density of the gas in the bubble, v is the radial velocity, p is the gas pressure, and k is the polytropic index (with $1 \leqslant k \leqslant \gamma$). A scaling argument for the neglect of viscosity can be found, for example, in Prosperetti *et al.* (1988). The validity of the polytropic approximation will be discussed later.

Prosperetti (1991) developed an asymptotic analysis of the Euler equations, including heat transfer, in the interior of oscillating bubbles. The small parameter is $M_0^2 \equiv (\omega R_0)^2\rho_0/p_0$, where ω is the driving frequency, R is the bubble radius, M is a Mach number, and the subscript 0 denotes an equilibrium quantity. The leading-order result of this asymptotic analysis is a solution featuring spatially uniform pressure, while the first correction corresponds to an inertially driven spatial non-uniformity in the pressure. As equilibrium quantities are used in the definition of the small parameter in the theory, it can be anticipated that the domain of application is limited to bubbles not far from equilibrium. In fact, Prosperetti himself writes that the results do not 'necessarily extend to the case of the catastrophic collapse of cavitation bubbles during which the radius can undergo an order-of-magnitude decrease'.

Motivated by this observation we search for an appropriate parameter that will serve to distinguish pressure non-uniformity in the case of violent collapses. We begin by assuming that pressure is spatially uniform, i.e. a function of time only

$$p=\bar{p}(t). \tag{2.4}$$

Now we shall examine the self-consistency of this assumption. From the polytropic relation (2.3) density also must be a function of time only. The total mass of the gas in the bubble is conserved; this leads to

$$\rho=\bar{\rho}(t)=\rho_0(R_0/R(t))^3. \tag{2.5}$$

We substitute this expression for ρ into the continuity equation (2.1), solve for the velocity field and obtain

$$\bar{v}=\frac{\dot{R}}{R}r. \tag{2.6}$$

Now we substitute (2.5) and (2.6) into the balance of radial momentum (2.2), and obtain an expression for the pressure gradient:

$$\frac{\partial p}{\partial r}=-\frac{\bar{\rho}\ddot{R}r}{R}. \tag{2.7}$$

This can be immediately integrated to obtain

$$p(r,t)=p_c(t)\left[1-\frac{1}{2}\frac{\bar{\rho}\ddot{R}R}{p_c}\left(\frac{r}{R}\right)^2\right]=p_c(t)\left[1-\frac{\gamma}{2}\epsilon_p\left(\frac{r}{R}\right)^2\right], \tag{2.8}$$

where $p_c(t) \equiv p(r=0,t)$, and we have defined the dimensionless quantity

$$\epsilon_p \equiv \frac{R\ddot{R}}{\bar{a}^2}, \tag{2.9}$$

with $\bar{a} \equiv \sqrt{\gamma p_c/\bar{\rho}}$. This demonstrates that the assumed solution of uniform pressure is only exactly self-consistent if the quantity ϵ_p, which may be regarded as a dimen-

sionless acceleration, is zero. One can expect it may be a good approximation if ϵ_p is small.

Next we need to check the continuity equation for self-consistency, as the assumption of uniform pressure led immediately to the result that density is also uniform. The polytropic relation relates the spatial gradient of density to that of the pressure as

$$\frac{1}{\rho}\frac{\partial \rho}{\partial r} = \frac{1}{k}\frac{1}{p}\frac{\partial p}{\partial r} \sim \frac{1}{k p_c}\frac{\bar{\rho}\ddot{R}r}{R}. \tag{2.10}$$

We compare the spatial density variation term to others in the continuity equation (2.1) and obtain

$$\frac{\dfrac{v}{\rho}\dfrac{\partial \rho}{\partial r}}{\min\left[\dfrac{1}{\rho}\dfrac{\partial \rho}{\partial t}, \dfrac{\partial v}{\partial r}, \dfrac{v}{r}\right]} \sim \frac{\bar{v}\dfrac{1}{kp}\dfrac{\partial p}{\partial r}}{\dot{R}/R} \sim \gamma \epsilon_p \frac{r^2}{R^2}. \tag{2.11}$$

Thus when ϵ_p is zero, the assumption of spatially uniform pressure also leads to exact self-consistency in the continuity equation.

Hence, the same dimensionless quantity ϵ_p must be zero for self-consistency of the balance of linear momentum and of the continuity equation. When the parameter ϵ_p is small but non-zero, and the other terms in these equations are not small, then uniform pressure and density are in error, but the errors are small.

This straightforward analysis forces us to confront the question of the relevance of the Mach number to the spatial uniformity of the pressure. Note that as long as $\dot{R} = \text{constant}$, $\epsilon_p = R\ddot{R}/a^2 = 0$ and (2.4), (2.5), (2.6) constitute an exact solution of the Euler equations. Theoretically one could set up a constant bubble wall velocity to obtain an arbitrarily large Mach number, yet the uniform pressure field is still a solution; however, we emphasize that the stability of (2.4), (2.5), (2.6) has not been verified. Nevertheless, we have found that in numerical simulations, a uniform pressure field is observed in collapses with $\dot{R} = \text{constant}$ and $M = \dot{R}/\bar{a}$ not small.

If we approach from a different perspective, the dimensionless quantity ϵ_p has an interesting physical interpretation. We can rewrite ϵ_p as the ratio of two time scales

$$\epsilon_p = \frac{\tau_1}{\tau_2}, \tag{2.12}$$

with $\tau_1 = R/\bar{a}$, $\tau_2 = \bar{a}/\ddot{R}$. We interpret τ_1 as the time scale for a disturbance to travel through the bubble radius, and τ_2 as a time scale associated with the bubble wall acceleration. This suggests that the uniformity of the pressure within the bubble is really determined by the *acceleration* of the wall. Even in the situation of a violent collapse with $\ddot{R}/\bar{a}$ being a very large quantity, the number τ_1 may be small enough in a minute bubble to make ϵ_p small – with fairly uniform pressure and density in the gas as the net result.

The quantity ϵ_p can also be understood from an acoustical point of view.† We define an acceleration time scale τ_a as $\tau_a^2 \equiv R/\ddot{R}$. A wavelength λ can then be defined as $\lambda^2 \equiv \bar{a}^2\tau_a^2 = \bar{a}^2 R/\ddot{R}$. The pressure field will be uniform if $R^2 \ll \lambda^2$, i.e. if $\epsilon_p \ll 1$.

A plot of the dimensionless quantity ϵ_p during a typical (violent) collapse is shown in figure 1. It is calculated *ex post facto* using (2.9), with the values of R, $\ddot{R}$ and $\bar{a} = \sqrt{\gamma p_c/\bar{\rho}}$ obtained from a full compressible Navier–Stokes calculation (DNS, see table 1) of the bubble interior (Storey & Szeri 1999, 2000). For the purpose of

† We thank an anonymous referee, who suggested the alternative understanding in this paragraph.

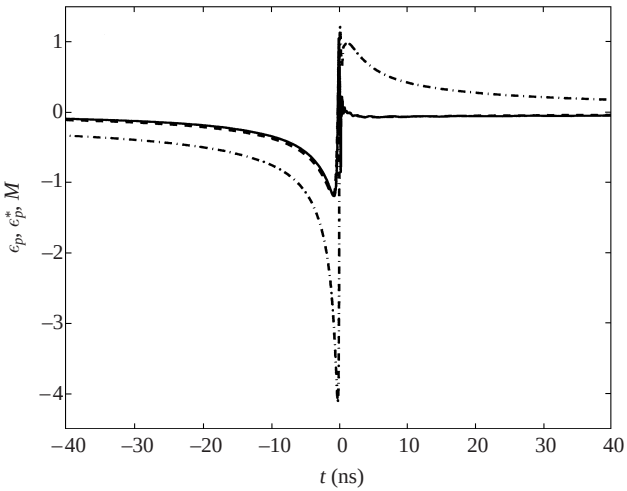

FIGURE 1. A comparison of ϵ_p (dashed curve, equation (2.9)), ϵ_p^* (solid, equation (2.14)) and the Mach number (dot-dashed), which demonstrates that the approximation ϵ_p can give information about pressure *non-uniformities* that agrees with DNS (ϵ_p^*). Meanwhile the Mach number exceeds unit magnitude over a time interval that appears to be not so well correlated with the pressure non-uniformity observed by DNS. The parameter values are the same as shown in table 1, case b, except that the dimensionless driving pressure amplitude is set to be $P_a = 1.25$.

Case	R_0 (μm)	T_0 (K)	P_a
a	4.5	298	1.1
b	4.5	298	1.2
c	4.5	298	1.3
d	4.5	278	1.2
e	4.5	308	1.2
f	4.5	318	1.2
g	2.5	298	1.2
h	6.5	298	1.2
i	8.5	298	1.2

TABLE 1. Parameter values for cases considered in the paper. For DNS, we make use of a full compressible Navier–Stokes simulation with convective/diffusive heat and mass transfer, phase change, and chemical reactions. For equation of state in the DNS, we use the Soave–Redlich–Kwong equation (Reid, Prausnitz & Poling 1987). R_0 is the ambient bubble radius, T_0 is the ambient temperature, and P_a is the dimensionless driving pressure amplitude. Other parameters are: driving frequency $f_d = 26\,500$ Hz, and ambient pressure $P_0 = 101.325$ kPa. The gas content is argon, with dynamic fraction of water vapour determined by evaporation/condensation/diffusion. Note that different R_0 and T_0 may result in different amounts of water vapour trapped in the bubble. For details of the numerical simulation see Storey & Szeri (2000).

comparison we also show the gas Mach number $M = \dot{R}/\bar{a}$, with the values of $\dot{R}$ and $\bar{a}$ from DNS as well. Finally, in order to verify that ϵ_p is indeed a suitable indicator for pressure inhomogeneity, we invert (2.8) formally to obtain

$$\epsilon_p = \frac{2}{\gamma}\left(1 - \frac{p}{p_c}\right) \Big/ \left(\frac{r}{R}\right)^2. \tag{2.13}$$

This expression can be evaluated at the bubble surface $r = R$, which yields

$$\epsilon_p^* = \frac{2}{\gamma}\left(1 - \frac{p_w}{p_c}\right). \tag{2.14}$$

Here the subscript w denotes a quantity evaluated at $r = R$, and we have distinguished ϵ_p^* from ϵ_p defined in (2.9) because we compute ϵ_p^* with the values of p_w and p_c from DNS instead. The result of this exercise is also shown in figure 1. It is clear that the dimensionless quantity ϵ_p obtained from (2.9) has a very similar value to the dimensionless centre-to-wall pressure difference measured in terms of ϵ_p^* using (2.14). As a hint of developments to come, this suggests that (2.8) is a fairly accurate representation of the spatially inhomogeneous pressure field in the bubble. To avoid confusion, although ϵ_p and ϵ_p^* are both calculated using DNS values, ϵ_p is a result we are testing against the 'real' pressure inhomogeneity measured by ϵ_p^*. Meanwhile changes in the Mach number seem not to be so well correlated with those in ϵ_p^*.

We make two further observations about the comparison between ϵ_p and ϵ_p^* in figure 1. First, the DNS includes both heat and mass transfer, while (2.8) is derived under the idealized model (2.1), (2.2), (2.3). Secondly, equation (2.8) was obtained while arguing that the uniform pressure approximation is approximately self-consistent when ϵ_p is small. However, as one observes in the figure, ϵ_p is not small. The situation depicted in figure 1 would appear to violate the ansatz of the arguments in two basic ways. Nevertheless, one observes that ϵ_p and ϵ_p^* are in close agreement.

In the following sections we study the reasons why the parameter ϵ_p and related quantities are accurate indicators of spatial inhomogeneity. Indeed, we can compute in terms of ϵ_p the departure of the pressure field from uniform, owing to inertial effects. Moreover, the quantity ϵ_p plays a role in assessing the onset and strength of wave-like motions in the gas.

3. Inertial departure from uniform pressure when ϵ_p = constant

In order to understand better the physical significance of the quantity ϵ_p, we first consider a situation where it arises rather naturally, albeit only as a constant. We have stated that when $\epsilon_p = 0$, then (2.4), (2.5), (2.6) comprise an exact solution to the Euler equations (2.1), (2.2), (2.3). In the case when ϵ_p is a finite constant, Chu (1996) has observed a 'similarity' structure in the gas dynamics; however, in that work he stops at the conclusion that ϵ_p must be a constant in order for the similarity structure to exist. The interested reader will note that in his equation (10), the first term is $R\ddot{R}/2h_c(t)$, expressed in terms of the enthalpy at the bubble centre $h_c(t)$. This is readily verified to be equivalent to the present ϵ_p. In this section we follow the analysis of Chu (1996), with the slight change to take into account the overall mass balance. However, we press on and develop an explicit set of similarity solutions.

In the following we assume that ϵ_p is constant. The first interesting observation is that, if the velocity possesses a linear form as in (2.6), then the continuity equation (2.1) admits a non-uniform density field

$$\rho(r,t) = \bar{\rho}(t)f(x) = \rho_0\left(\frac{R_0}{R(t)}\right)^3 f\left(\frac{r}{R(t)}\right), \tag{3.1}$$

where $x \equiv r/R(t)$, and $\bar{\rho}(t)$ is as defined in (2.5). Next, we assume that the velocity and density fields are as given in (2.6) and (3.1) and substitute them into the balance of radial momentum (2.2); we finally integrate from 0 to r to obtain an expression

for the pressure:

$$p(r,t) = p_c(t)\left(1 - \gamma\epsilon_p \int_0^{x=r/R} yf(y)\,\mathrm{d}y\right). \tag{3.2}$$

This expression for the pressure is in turn substituted into the energy equation to obtain a second expression for density:

$$\rho(r,t) = \rho_c(t)\left(1 - \gamma\epsilon_p \int_0^{x} yf(y)\,\mathrm{d}y\right)^{1/k}, \tag{3.3}$$

where $\rho_c(t) \equiv \rho(r=0,t)$. Evidently, the two expressions for the density field (3.1) and (3.3) must be equal for a self-consistent solution. This leads directly to

$$\bar{\rho}(t)f(x) = \rho_c(t)\left(1 - \gamma\epsilon_p \int_0^{x} yf(y)\,\mathrm{d}y\right)^{1/k}, \tag{3.4}$$

or, in fact, the nonlinear integral equation

$$f(x) = f(0)\left(1 - \gamma\epsilon_p \int_0^{x} yf(y)\,\mathrm{d}y\right)^{1/k}. \tag{3.5}$$

In the latter we have made use of $\rho_c(t) = \bar{\rho}(t)f(0)$. Finally we recast this integral equation as a differential equation to enable a solution; differentiation yields

$$-\frac{kf(x)^{k-2}f'(x)}{f(0)^k} = \gamma\epsilon_p x. \tag{3.6}$$

The ODE can be solved in closed form. When $k = \gamma$ one obtains

$$f(x) = f(0)\left(1 - \frac{(\gamma-1)}{2}\epsilon_p f(0)x^2\right)^{1/(\gamma-1)}, \tag{3.7}$$

hence

$$\rho(r,t) = \bar{\rho}(t)f(0)\left(1 - \frac{(\gamma-1)}{2}\epsilon_p f(0)x^2\right)^{1/(\gamma-1)} \tag{3.8}$$

and

$$p(r,t) = p_c(t)\left(1 - \frac{(\gamma-1)}{2}\epsilon_p f(0)x^2\right)^{\gamma/(\gamma-1)}; \tag{3.9}$$

while if $k = 1$ one finds an exponential form of $f(x)$:

$$f(x) = f(0)\exp(-\tfrac{1}{2}\gamma\epsilon_p f(0)x^2), \tag{3.10}$$

which yields

$$\rho(r,t) = \bar{\rho}(t)f(0)\exp(-\tfrac{1}{2}\gamma\epsilon_p f(0)x^2) \tag{3.11}$$

and

$$p(r,t) = p_c(t)\exp\left(-\tfrac{1}{2}\gamma\epsilon_p f(0)x^2\right). \tag{3.12}$$

The only quantity that remains to be determined to fix the solution is $f(0)$. This can be found from the overall mass conservation of the bubble, i.e.

$$\int_0^R \bar{\rho}f(x)4\pi r^2\,\mathrm{d}r = \tfrac{4}{3}\pi R^3\bar{\rho}. \tag{3.13}$$

In general this integral must be carried out numerically. However in the case of

present interest (see figure 1), where ϵ_p is a small quantity, we can approximate $f(0)$ by an asymptotic expansion.† We carry out the calculation for $k = \gamma$, as follows. First, we expand equation (3.8) assuming $\epsilon_p f(0) \ll 1$ and obtain

$$\rho(r,t) \approx \bar{\rho}(t) f(0) \left(1 - \tfrac{1}{2}\epsilon_p f(0) x^2 + \frac{2-\gamma}{8}\epsilon_p^2 f(0)^2 x^4 + \cdots\right). \tag{3.14}$$

Here we keep only terms to the second order. With this approximation we can then explicitly evaluate equation (3.13) to obtain

$$f(0) - \tfrac{3}{10}\epsilon_p f(0)^2 + \tfrac{3}{56}(2-\gamma)\epsilon_p^2 f(0)^3 = 1. \tag{3.15}$$

Now we assume that $f(0)$ takes the asymptotic form

$$f(0) = 1 + A\epsilon_p + B\epsilon_p^2 + \cdots, \tag{3.16}$$

where A and B are constants to be determined. We substitute it into equation (3.15), equate like powers of ϵ_p and obtain

$$f(0) = 1 + \tfrac{3}{10}\epsilon_p + \frac{102 + 75\gamma}{1400}\epsilon_p^2 + \cdots. \tag{3.17}$$

Similarly, we can carry out the calculation for the case $k = 1$. To a first-order approximation (which is sufficient in most of the cases), we have a unified formula for $f(0)$ for both $k = 1$ and $k = \gamma$ as

$$f(0) = 1 + \frac{3\gamma}{10k}\epsilon_p + \cdots. \tag{3.18}$$

In the same spirit, one can simplify (3.8) and (3.9) by Taylor expansion for small ϵ_p using (3.18), to obtain

$$\rho(r,t) = \bar{\rho}\left[1 + \frac{\gamma}{2k}\epsilon_p(\tfrac{3}{5} - x^2)\right], \tag{3.19}$$

$$p(r,t) = p_c(t)(1 - \tfrac{1}{2}\gamma\epsilon_p x^2). \tag{3.20}$$

Note that (3.20) has appeared before as (2.8).

Despite the fact that (3.18), (3.19), (3.20) have been obtained in an argument where ϵ_p is supposed to be small, the formulae are quite accurate up to $|\epsilon_p| \sim 1$, owing to the smallness of the remainder in the expansion. (As an illustration, consider $\epsilon_p = -1$. From the fully nonlinear expressions (3.13), (3.8), (3.9) one obtains $f(0) = 0.8$, $\rho_w/\bar{\rho} = 1.14$, and $p_w/p_c = 1.81$. From the small-ϵ_p approximations (3.18), (3.19), (3.20), one finds $f(0) = 0.7$, $\rho_w/\bar{\rho} = 1.2$, and $p_w/p_c = 1.83$. For further illustration, see figure 2.) Finally, we note that both the near-adiabatic and near-isothermal formulae deliver the same expressions for small ϵ_p. Thus (3.19) and (3.20) may be used for both cases.

A further observation concerning (3.20) is that it is equivalent to the Bernoulli equation

$$p(r,t) = p_c(t) - \bar{\rho}(t)\left(\frac{\partial\phi}{\partial t} + \tfrac{1}{2}|\nabla\phi|^2\right), \tag{3.21}$$

where

$$\phi \equiv \tfrac{1}{2}R\dot{R}x^2 \tag{3.22}$$

is the corresponding velocity potential of (2.6). Hence if one is concerned only with

† We thank an anonymous referee, who suggested the development shown in this paragraph.

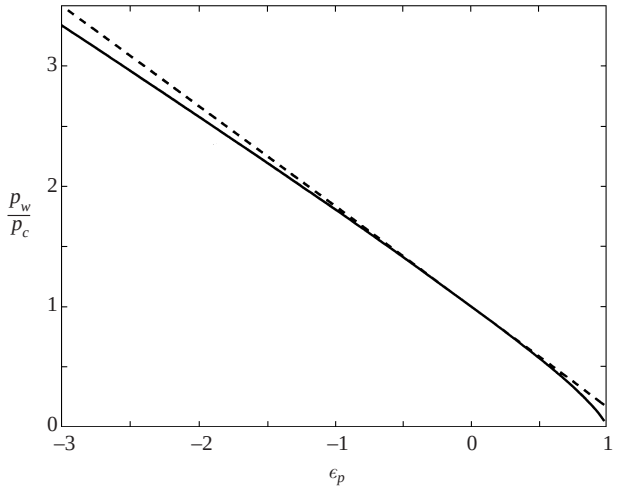

FIGURE 2. A comparison of p_w/p_c determined from (3.9) (solid) and from the simpler approximation (3.20) (dashed) over a wide range of values of ϵ_p.

the pressure field, a uniform density $\bar{\rho}(t)$ can be used for inertia to give a fair approximation.

4. Inertial departure from uniform pressure when ϵ_p is time dependent

Now we have an exact solution to the governing equations (2.1), (2.2), (2.3) under the condition that $\epsilon_p =$ constant. A natural question is, is this solution useful in the case of interest, where ϵ_p is a function of time?

We consider again the violently collapsing bubble of figure 1. Except during the slow expansion and the after-bounces where ϵ_p is almost zero (not shown), it varies considerably with time. However, if we naively use a time-dependent $\epsilon_p(t)$ (calculated with (2.9) *ex post facto* from DNS) in (3.8), (3.9), i.e. in

$$\rho(r,t) = \bar{\rho}(t)f(0)\left(1 - \frac{\gamma-1}{2}\epsilon_p(t)f(0)x^2\right)^{1/(\gamma-1)}, \tag{4.1}$$

$$p(r,t) = p_c(t)\left(1 - \frac{\gamma-1}{2}\epsilon_p(t)f(0)x^2\right)^{\gamma/(\gamma-1)}, \tag{4.2}$$

we observe a fairly close agreement with the DNS calculation of the pressure field, as shown in figures 3 and 4. These results encompass a brief period of time around the minimum radius, where $k = \gamma$ is valid; ϵ_p is otherwise small. Thus in the following we shall phrase the discussion in terms of the case $k = \gamma$, but the analysis and conclusions extend to the case $k = 1$ as well.

As suggested by examination of figures 3 and 4, the inertial departure from uniform pressure developed following the assumption of constant ϵ_p evidently applies equally well to the case where ϵ_p varies with time. The question then is, why is the approximation accurate, and when can it be expected to remain so?

In order to investigate the errors in the approach, let us suppose that ϵ_p is a 'slow' function of time, where the meaning of 'slow' will emerge in due course. The density

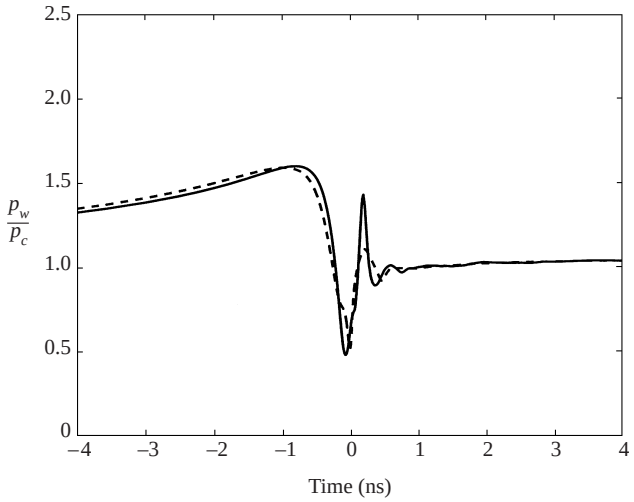

FIGURE 3. In the case of the same parameter values as figure 1, but on a much smaller time scale, there is close agreement between p_w/p_c from DNS (dashed) and the approximation (4.2) (solid, where ϵ_p is calculated with the values of R, $\ddot{R}$ and $\bar{a}$ from DNS) for the critical interval around the major collapse.

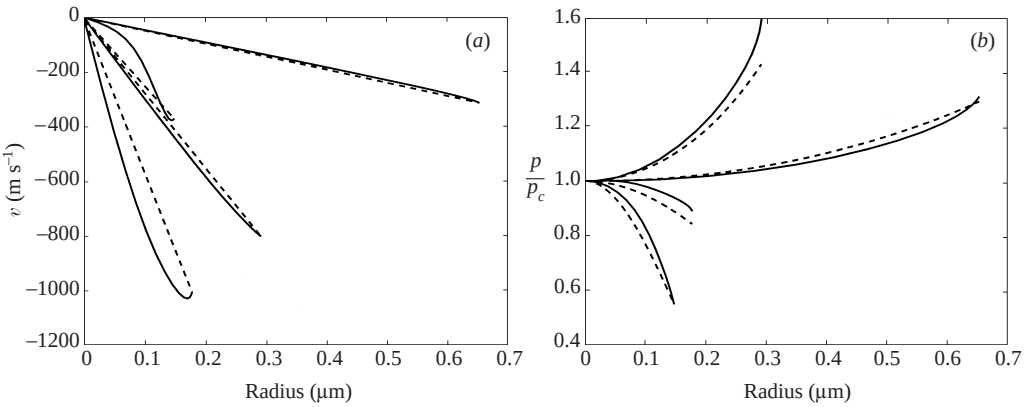

FIGURE 4. Snapshots of (*a*) velocity and (*b*) pressure fields at times relative to the time of minimum radius for the bubble in figure 1. The solid curves are from DNS and the dashed curves are the approximations (4.2), (2.6).

and pressure fields (4.1), (4.2) may be written in the form

$$\rho(r,t) = \bar{\rho}(t) f(\epsilon_p(t), x), \tag{4.3}$$

$$p(r,t) = p_c(t) g(\epsilon_p(t), x). \tag{4.4}$$

When ϵ_p is no longer constant, we can expect a deviation from linearity in r in the velocity field as well. Hence we write

$$v(r,t) = \bar{v}(1 + \epsilon_v(r,t)), \tag{4.5}$$

where $\bar{v}$ is as given in (2.6). The strategy now will be to determine when (4.3), (4.4), (4.5) are self-consistent. We shall observe that they are not, in general, and develop a convenient measure for the error. To begin, we substitute (4.3), (4.5) into the continuity

equation to obtain

$$\bar{\rho}(t)\frac{\partial f}{\partial \epsilon_p}\dot{\epsilon}_p + \frac{1}{r^2}\frac{\partial}{\partial r}[r^2\rho\bar{v}\epsilon_v] = 0. \tag{4.6}$$

This is integrated to obtain

$$\epsilon_v(r,t) = -\frac{1}{\rho\bar{v}r^2}\int_0^r \bar{\rho}(t)\frac{\partial f}{\partial \epsilon_p}\dot{\epsilon}_p r^2 \mathrm{d}r. \tag{4.7}$$

Now we shall assume that ϵ_v is small, in accordance with the assumption of 'slow' changes in ϵ_p; note that $\epsilon_v = 0$ for $\dot{\epsilon}_p = 0$. To find the error associated with the pressure solution, we substitute (4.3), (4.7) into the balance of radial momentum and integrate from 0 to r to obtain

$$p(r,t) = p_c(t) - \int_0^r \rho\left(\frac{\mathrm{D}\bar{v}}{\mathrm{D}t} + \frac{\partial(\bar{v}\epsilon_v)}{\partial t} + \frac{\partial(\bar{v}^2\epsilon_v)}{\partial r}\right)\mathrm{d}r. \tag{4.8}$$

Here we have neglected higher-order terms in ϵ_v. If we substitute (4.4) for $p(r,t)$ into this equation, after cancellations we are left with a residual

$$0 = -\int_0^r \rho\left(\frac{\partial(\bar{v}\epsilon_v)}{\partial t} + \frac{\partial(\bar{v}^2\epsilon_v)}{\partial r}\right)\mathrm{d}r. \tag{4.9}$$

For convenience we shall define a new dimensionless error measure based on this residual as

$$\epsilon_{error} = \frac{1}{p_c}\int_0^R \rho\left|\frac{\partial(\bar{v}\epsilon_v)}{\partial t} + \frac{\partial(\bar{v}^2\epsilon_v)}{\partial r}\right|\mathrm{d}r. \tag{4.10}$$

Note we have used the absolute value in the integrand, to prevent cancellation of the accumulative error along with the integration. Evidently, if ϵ_{error} is small, then equations (4.3), (4.4), (2.6) serve as good approximation to the solution of the Euler equations (2.1), (2.2), (2.3). This we shall take as a definition of 'slow' changes in $\epsilon_p(t)$. To proceed any further, owing to the complicated algebraic dependence of $f(0)$ on ϵ_p, (4.7), (4.10) must be evaluated numerically.

However, if we make use of (3.19), (3.20) but with $\epsilon_p(t)$ time dependent, it is possible to obtain explicit, convenient expressions for both ϵ_v and ϵ_{error}. The integral in expression (4.7) may be evaluated as

$$\epsilon_v = -\frac{\gamma}{10k}\dot{\epsilon}_p\frac{R}{\dot{R}}(1-x^2). \tag{4.11}$$

Note that the apparent singularity in ϵ_v when $\dot{R} \to 0$ is an artifact of the form assumed rather than anything physical. (See (4.5), in which $\bar{v} = \dot{R}x$.) The dimensionless error estimate is

$$\epsilon_{error} \equiv \frac{p_{error}}{p_c} = \frac{\bar{\rho}R}{p_c}\left|\frac{\gamma}{2k}\left(\frac{1}{20} + \frac{\gamma\epsilon_p}{150k}\right)\left(2\dot{R}\dot{\epsilon}_p + R\ddot{\epsilon}_p\right)\right|. \tag{4.12}$$

For the case of figures 1 and 3–4, we show the corresponding ϵ_{error} in figure 5. Except for a brief moment around the minimum radius, ϵ_{error} is small, although ϵ_p is not always small. Thus we have verified that (4.1), (4.2), (2.6) can indeed be a good approximation to the solution of the Euler equations (2.1), (2.2), (2.3) even when ϵ_p is time dependent and not small.

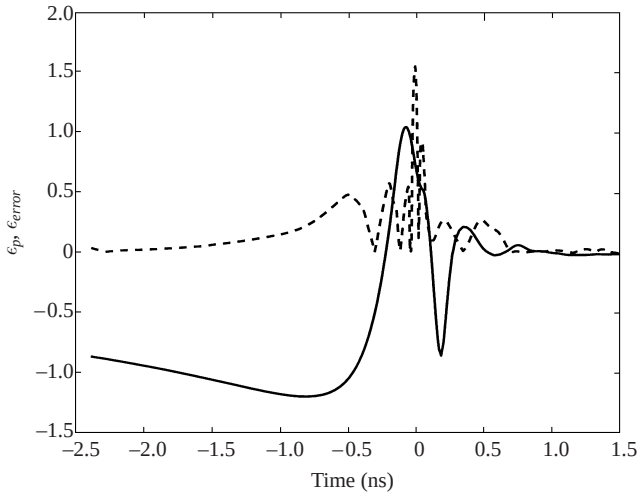

FIGURE 5. The error measure ϵ_{error} (dashed) for the bubble of figure 1. For reference also plotted is ϵ_p (solid). As in the previous figures both ϵ_{error} and ϵ_p are obtained using DNS values in the expressions (4.12) and (2.9).

5. Influence of heat transfer

An unresolved point is that despite the use of the polytropic equation (2.3), figure 3 has shown surprisingly good agreement between the approximation (4.2) and DNS. This is true notwithstanding the fact that in the latter both heat and mass transfer are included. In this section we consider the reasons for this.

When a bubble undergoes a violent collapse, the gas in the bubble is rapidly heated. The temperature at the centre can rise by more than an order of magnitude, while the temperature at the bubble interface remains much closer to ambient owing to the large heat capacity of the liquid. A thin thermal boundary layer forms in the gas near the bubble wall while the gas deeper in the interior typically has a fairly uniform temperature. There is vigorous heat flux during the late stages of collapse, but little heat is lost compared to the amount that is stored in the bubble. The interior temperature remains uniform because the collapse is so rapid that heat in the interior has insufficient time to escape through the bubble wall (Hickling 1963; Storey & Szeri 2001). In the boundary layer the density increases sharply, and velocity correspondingly departs from linearity. In spite of these deviations due to the thermal behaviour, the analysis of the foregoing sections is still valid in the bubble interior, owing to the fact that (2.3) is approximately satisfied there.

To further complicate matters, water is constantly evaporating and condensing at the bubble wall – an effect that has been neglected in the present analysis. Instead, we have assumed that the mass of the bubble contents is constant. This is a valid assumption over the time scale of interest around a violent collapse as shown in Storey & Szeri (2000). To account for vapour, we can simply define $\bar{\rho}(t)$ to be the total mass of gas and vapour divided by the volume, and the analysis thus follows.

We note that in (3.2), the pressure field involves the integral of density times acceleration. Although there is a significant deviation of the density field from our idealization (4.1), the average density $\bar{\rho}(t)$ is accurate. We find that the influence of density variation in the pressure formula (4.2) is suppressed through integration, owing to the relatively small thickness of the thermal boundary layer. In figure 6 we

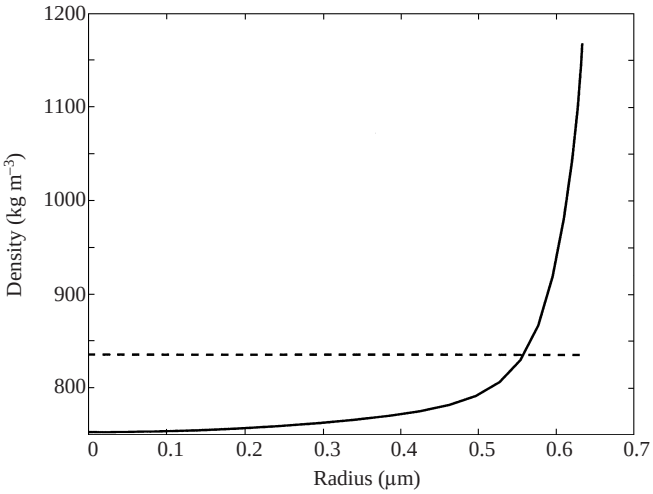

FIGURE 6. A typical density profile in a violently collapsing bubble (solid curve). The dashed line is the averaged density $\bar{\rho}(t) = \rho_0(R/R_0)^{-3}$. This is case c of table 1 at time $t = 0$ ns.

show a typical density distribution within the bubble along with the average density. We find that carrying out the integral for pressure (3.2) using the true density field or the average results only in a 2% error in this typical case.

Evidently, the assumption of an average density suffices to provide a rather good estimate for the integral in equation (3.2). As this result has been verified well by extensive comparisons with DNS, we assert (but without proof, nor is it necessarily true in all circumstances) that in the near-adiabatic limit although ρ and T (temperature) may show significant non-homentropic behaviour, the dynamical fields v and p in (2.6) and (4.2) are good approximations; that is to say, the latter are only weakly coupled with the former. The physical reason is that the pressure inhomogeneity is mainly driven by inertia.

In figure 7 we show several comparisons of ϵ_p (the approximation (2.9)) to ϵ_p^* (the actual pressure non-uniformity (2.14)) to support this point. The plots correspond to a variety of cases. In all the cases we have the same parameter values as in figures 1 and 3–5, but we vary R_0, T_0 and P_a as listed in table 1. Note that we have focused on the parameter range of tiny bubbles and high-amplitude forcing, which represents the most violent collapses allowed for stable bubbles. (For the stable parameter range see e.g. Hilgenfeldt, Lohse & Brenner 1996.)

The only cases where the approximation deviates from the numerics significantly are (c) and (f), although it is perhaps difficult to see on the time interval shown. In these two calculations the exceptionally violent collapse traps large amounts of vapour. As a consequence of the associated decrease in the ratio of specific heats, the gas is more easily compressed. The gas dynamics briefly features strong wave-like motions and (4.2) is (briefly) not applicable. This topic will be further explored following a discussion of the accuracy and validity of the RPE vis-à-vis the assumption of uniform pressure.

Interested readers are referred to Prosperetti *et al.* (1988) (equation (14)) for a reduced model with non-uniform temperature field, a corresponding correction to the linear velocity field due to heat transfer, and employing an assumption of uniform pressure. A further improvement of the present model could be obtained following those arguments, where we use the non-uniform pressure developed in this work

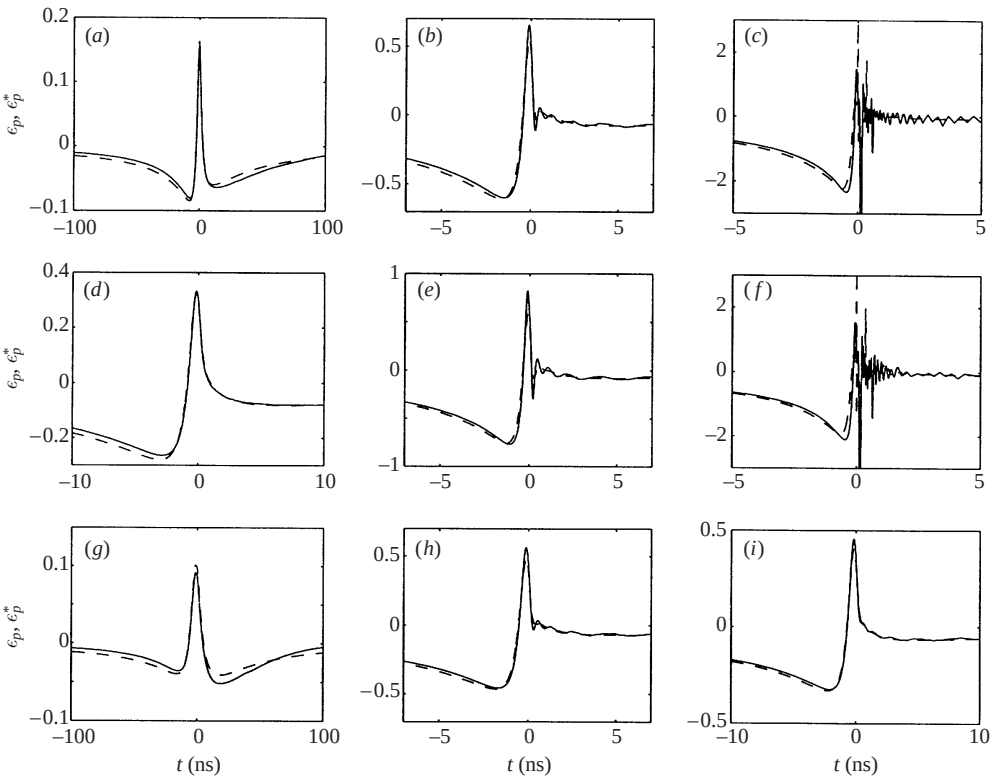

FIGURE 7. Various case studies which illustrate the agreement between the approximation (dashed curve, ϵ_p) and DNS (solid curve, ϵ_p^*). The calculations are carried out the same way as in figure 1. In each plot the abscissa is time $t = 0$ ns; note the scales differ sometimes by orders of magnitude from case to case. The corresponding parameter values are given in table 1.

instead of a uniform one. In this way, we could assess the influence of pressure inhomogeneity on the temperature field (especially the maximum temperature, which is of most interest). We leave this for future work.

6. The Rayleigh–Plesset equation

We now have knowledge of the pressure inhomogeneity within sufficiently violently collapsing bubbles. Thus, we are in a position to assess the validity and accuracy of the assumption of uniform pressure to close the RPE. We will consider also the importance of the inertial departure from uniform pressure on bubble dynamics.

We begin with any suitable version of the Rayleigh–Plesset equation, for example, that by Lofstedt, Barber & Putterman (1993), which is written as

$$-R\ddot{R}\left(1-\frac{2\dot{R}}{c}\right)-\frac{3}{2}\dot{R}^2\left(1-\frac{4}{3}\frac{\dot{R}}{c}\right)+\frac{1}{\rho}\left(P(R,t)-P_a(0,t)-P_0\right)$$
$$+\frac{R}{\rho c}\left(\frac{\mathrm{d}P(R,t)}{\mathrm{d}t}-\frac{\mathrm{d}P_a(0,t)}{\mathrm{d}t}\right)=0, \quad (6.1)$$

where

$$P(R,t)+\frac{4\mu\dot{R}}{R}+\frac{2\sigma}{R}=P_g(R,t) \quad (6.2)$$

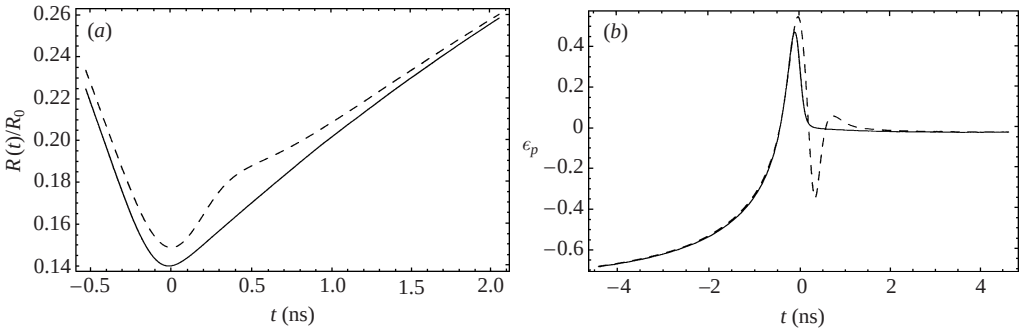

FIGURE 8. A comparison of a uniform-pressure RPE solution (solid curve, equation (6.3)) and an inertially corrected RPE solution (dashed, equation (6.4)). (*a*) A plot of the radius versus time around the minimum radius; a small bump just after the minimum radius distinguishes the inertially corrected model. This is better seen in (*b*) where only the inertially corrected RPE solution captures the overshoot in acceleration after the major collapse. This overshoot has been observed before only in DNS. The parameter values are: ambient radius $R_0 = 4\,\mu\text{m}$, pressure amplitude $P_a = 1.4\,\text{atm}$ and frequency $f = 26\,500\,\text{Hz}$.

and

$$P_g(R) = \frac{P_0 R_0^{3k}}{(R^3 - a^3)^k}. \tag{6.3}$$

By suitable, we mean that the correction for liquid compressibility has been included. Prosperetti (1999) has shown that various forms correct to order Ma_l in the liquid Mach number are equivalent. As is the usual practice, we utilize a uniform gas pressure P_g. We wish to know what is the consequence of using instead the inertial correction (4.2) in place of the uniform pressure to close the RPE.

We simply take the uniform van der Waals pressure (6.3) as our $p_c(t)$, and use (3.20) to amend the gas pressure on the bubble wall to read

$$P_g(R) = \frac{P_0 R_0^{3k}}{(R^3 - a^3)^k}\left(1 - \frac{\gamma}{2}\epsilon_p\right). \tag{6.4}$$

We note that ϵ_p is a function of $\ddot{R}$, hence (6.1) becomes third order and we must add $\ddot{R}(t=0) = 0$ as an additional initial condition. The numerical integration leads to the dashed curve in figure 8(*a*), which we compare to the uniform pressure RPE (solid curve). A small bump is clearly seen immediately after the minimum radius in the inertially corrected pressure simulation, but not in the uniform pressure solution. This bump has been observed before only with full numerical simulation of the bubble interior as in Vuong & Szeri (1996). Otherwise, the two solutions, with and without the inertial pressure correction, are nearly identical.

A more sensitive discrimination is to plot $\epsilon_p(t)$ calculated with (4.2) using $R(t)$ from: (i) the homogeneous pressure RPE, and (ii) from the inertially corrected RPE; this is shown in figure 8(*b*). One observes that the inertial pressure correction in the RPE captures the characteristic overshoot visible in the DNS calculations in figure 7 (solid lines). This is further confirmation that (4.2) successfully captures the departure from uniform pressure.

Notwithstanding this interesting observation, one would be correct to conclude from figure 8 that, except for the small detail around the minimum radius, the uniform-pressure RPE works just as well. Thus the RPE is accurate for much more strongly collapsing bubbles than was previously thought. The uniform-pressure

assumption, although invalid on physical grounds when the bubble collapses with sufficient violence, serves well as far as the accuracy of the $R(t)$ curve is concerned.

7. Characterization of violent collapses and validity of the RPE

Now we summarize the foregoing development, and our experience with DNS, for practical use in general bubble dynamics. When a bubble suddenly expands or shrinks, a pressure disturbance is initiated at the bubble wall and propagates into the interior as a compression or rarefaction wave; the relative magnitude is given by the dimensionless estimate

$$\frac{\partial p^*}{\partial r^*} \sim -\frac{\bar{\rho}}{p_c}\ddot{R}R = -\gamma\epsilon_p, \tag{7.1}$$

where $p^* \equiv p/p_c$, $r^* \equiv x = r/R(t)$. The time it takes for such a disturbance to sweep through the bubble (roughly) is τ_1 in (2.12).

It is possible to divide the ensuing behaviour into three regimes, as follows.

(i) When both ϵ_p and ϵ_{error} are small, the disturbances are insignificant; the pressure field is almost spatially uniform.

(ii) When ϵ_p is not small but ϵ_{error} is small, the pressure possesses an essential, inertially driven spatial inhomogeneity, given by the approximation (4.2). (In most cases of interest (3.20) is sufficient.) Although in DNS one may observe slight wave-like gas dynamics in addition to the inertially driven inhomogeneity of (4.2), that equation serves as good global approximation.

(iii) Finally, when there is a rapid change in ϵ_p, designated by significant growth in ϵ_{error}, there is a strong wave-like character to the gas dynamics in addition to the inertially driven inhomogeneity of (4.2). The fate of such waves and their potential evolution into shocks can be analysed using a local expansion technique as in Lin & Szeri (2001).

The case we examined in figures 1–5 serves as a good illustration of type (i) and (ii) behaviour. In figure 5 although ϵ_{error} increases briefly, this is insufficient to signify strong wave-like gas dynamics, as one can see in figure 4. In the cases (excluding *c* and *f*) of figure 7, the pressure field possesses an essential inhomogeneity without significant wave-like motion in the gas; hence the pressure field is accurately approximated by (4.2).

It is in cases (*c*) and (*f*) of figure 7 where we observe significant wave-like gas dynamics, i.e. type (iii) behaviour. In figure 9(*a*), we have plotted ϵ_{error} for case 7(*c*) to determine the accuracy of (4.2). One observes that where ϵ_{error} grows, wave-like motions become evident in the pressure field (figure 9*b*); this leads to a deviation from the simple form of (4.2).

Finally, we note that in all three regimes (i–iii), the assumption of uniform pressure in the RPE gives quite accurate solutions for $R(t)$, although only in regime (i) is the assumption valid on physical grounds. In regime (i) (e.g. figure 7, cases *a* and *g*), the pressure field within the collapsing bubble is uniform to a high degree of accuracy. In regime (ii) (e.g. figure 7, cases *b*, *d*, *e*, *h* and *i*), the pressure field is essentially non-uniform, with only minor wave-like disturbances superposed on (4.2). However, as we have earlier discussed in § 6, this inhomogeneity only has an effect on $R(t)$ in the smallest details immediately following a strong collapse. In regime (iii) (e.g. figure 7, cases *c* and *f*), the approximation (4.2) loses its validity in the face of strong wave-like motions in the gas. Upon close examination (4.2) is found to be an over-prediction of the centre-to-wall pressure difference. This is because the wave-like motions in the

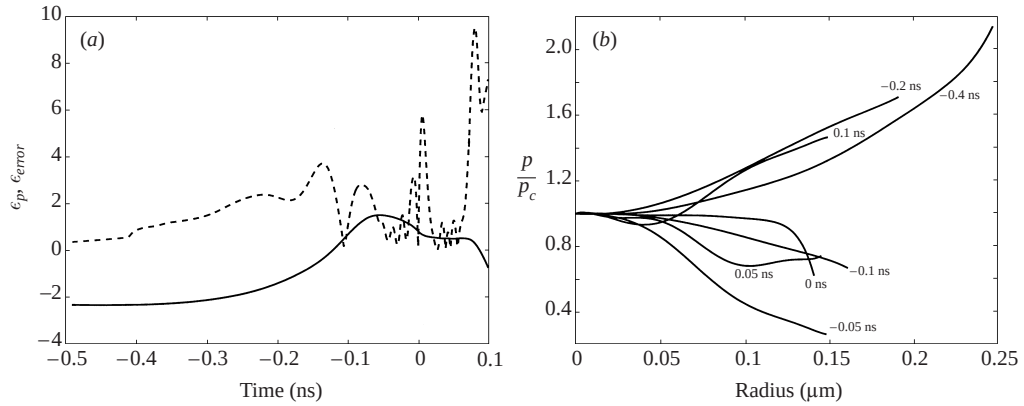

FIGURE 9. Dynamics near a very violent collapse, in which significant wave-like motions in the gas ensue. (*a*) A plot of ϵ_p (solid) and ϵ_{error} (dashed), calculated *ex post facto* using DNS values. The latter becomes large indicating the inaccuracy of the approximation (4.2). (*b*) Corresponding snapshots of the pressure field obtained by DNS.

gas always serve to ameliorate the centre-to-wall pressure difference. Even in regime (iii), the uniform-pressure RPE only misses the detail of the tiny bounce after the minimum radius of a strong collapse, which is on the time scale of hundreds of picoseconds. Although the uniform-pressure assumption is far from valid in regime (iii), the solution $R(t)$ of the uniform-pressure RPE is accurate except for the tiny bounce of § 6.

8. Conclusion

The present work has been a study of the self-consistency of the assumption of spatially uniform pressure within a bubble, which is commonly employed to close the Rayleigh–Plesset equation. We have developed the following results.

The natural parameter to use in evaluation of the uniform-pressure assumption in violent collapses is the parameter $\epsilon_p(t)$ and not the gas Mach number.

An approximation was developed for the internal pressure field, which is quite accurate when tested against DNS for bubble collapses without strong wave-like motions in the gas. This led to an error estimate ϵ_{error} associated with the uniform-pressure approximation. Together, ϵ_p and ϵ_{error} can be used to distinguish between several regimes of behaviour.

It was found that when present, spatial non-uniformity of the pressure within the bubble does not have a great influence on the accuracy of solutions $R(t)$ of the uniform-pressure RPE. The range of application of the RPE is thus extended to the regime of very strongly collapsing bubbles.

Our arguments have, of necessity, been motivated by physical intuition supplemented by the constraints of self-consistency. The latter fall into the category of only necessary conditions but not sufficient conditions; hence, where possible, we have appealed to direct numerical solutions to illustrate – and perhaps help to justify – the further development of the theory.

Support for this work was provided, in part, by the National Science Foundation and by the Lawrence Livermore National Laboratory. A. J. S. would like to thank the Alexander von Humboldt Foundation for the award of a Research Fellowship and Professor W. Lauterborn for hosting a pleasant stay in Göttingen.

REFERENCES

Chu, M.-C. 1996 The homologous contraction of a sonoluminescing bubble. *Phys. Rev. Lett.* **76**, 4632–4635.

Greenspan, H. P. & Nadim, A. 1993 On sonoluminescence of an oscillating gas bubble. *Phys. Fluids* A **5**, 1065–1067.

Hammer, D. & Frommhold, L. 2001 Sonoluminescence: how bubbles glow. *J. Mod. Optics* **48**, 239–277.

Hickling, R. 1963 Effects of thermal conduction on sonoluminescence. *J. Acoust. Soc. Am.* **35**, 967–974.

Hilgenfeldt, S., Lohse, D. & Brenner, B. P. 1996 Phase diagrams for sonoluminescing bubbles. *Phys. Fluids* **8**, 2808–2826.

Kwak, H.-Y. & Na, J. H. 1997 Physical processes for single bubble sonoluminescence. *J. Phys. Soc. Japan* **66**, 3074–3083.

Lin, H. & Szeri, A. J. 2001 Shock formation in the presence of entropy gradients. *J. Fluid Mech.* **431**, 161–188.

Lofstedt, R., Barber, B. P. & Putterman, S. J. 1993 Toward a hydrodynamic theory of sonoluminescence. *Phys. Fluids* A **5**, 2911–2928.

Prosperetti, A. 1991 The thermal behavior of oscillating gas bubbles. *J. Fluid Mech.* **222**, 587–616.

Prosperetti, A. 1999 Old fashioned bubble dynamics. In *Sonochemistry and Sonoluminescence*. NATO ASI Series C524 (ed. L. A. Crum, *et al.*), pp. 39–62. Kluwer.

Prosperetti, A., Crum, L. A. & Commander, K. W. 1988 Nonlinear bubble dynamics. *J. Acoust. Soc. Am.* **83**, 502–513.

Putterman, S. J., Evans, P. G., Vazquez, G. & Weninger, K. R. 2001 Is there a simple theory of sonoluminescence? *Nature* **409**, 782–783.

Reid, R. C., Prausnitz, J. M. & Poling, B. E. 1987 *Properties of Gases and Liquids*. McGraw-Hill.

Storey, B. D. & Szeri, A. J. 1999 Mixture segregation within sonoluminescence bubbles. *J. Fluid Mech.* **396**, 203–221.

Storey, B. D. & Szeri, A. J. 2000 Water vapour, sonoluminescence and sonochemistry. *Proc. R. Soc. Lond.* A **456**, 1685–1709.

Storey, B. D. & Szeri, A. J. 2001 A reduced model of cavitation physics for use in sonochemistry. *Proc. R. Soc. Lond.* A **457**, 1685–1700.

Trilling, L. 1952 The collapse and rebound of a gas bubble. *J. Appl. Phys.* **23**, 14–17.

Vuong, V. Q. & Szeri, A. J. 1996 Sonoluminescence and diffusive transport. *Phys. Fluids* **8**, 2354–2364.

Vuong, V. Q., Szeri, A. J. & Young, D. A. 1999 Shock formation within sonoluminescence bubbles. *Phys. Fluids* **11**, 10–17.